Internal-Rotation in Hydrogen Peroxide: The Far-Infrared Spectrum and the Determination of the Hindering Potential*

ROBERT H. HUNT,† ROBERT A. LEACOCK,‡ C. WILBUR PETERS, AND KARL T. HECHT
The Harrison M. Randall Laboratory of Physics, The University of Michigan, Ann Arbor, Michigan

(Received 29 September 1964)

The torsional oscillation between the two OH groups of the hydrogen peroxide molecule is investigated through a study of the far-infrared absorption spectrum of the molecule. A 1-m-focal-length vacuum grating monochromator was used to scan the region from 15 to 700 cm^{-1} with an average resolution of 0.3 cm^{-1}. The observed spectrum contains seven perpendicular-type bands of which only the Q branches are resolved. The centers of the seven bands are at 11.43, 116.51, 198.57, 242.76, 370.70, 521.68, and 557.84 cm^{-1}. These bands result from transitions between different states of the internal rotation and their identification makes it possible to construct the internal-rotation energy level scheme through the first five excited states. Relative to the torsional ground state, these levels occur at 11.43, 254.2, 370.7, 569.3, and 775.9 cm^{-1}.

A theory of internal rotation in the hydrogen peroxide molecule is developed for use in the analysis of the far-infrared spectra. In this theory, the Hamiltonian is constructed assuming all structural distances and angles fixed except the dihedral angle x defining the relative position of the two OH bars. By the use of a contact transformation the Hamiltonian is put in the form H (asymmetric top) +H(internal rotation) where the interaction between the internal and over-all rotations arises through the x dependence of the inertial parameters of H(asymmetric top). It is assumed that the relative position of the two OH bars is governed by a potential-energy function of the form $V(x)=V_1\cos x+V_2\cos 2x+V_3\cos 3x$. The internal-rotation wave equation $[\alpha p_x^2+V(x)]M(x)=\mathrm{EM}(x)$ is solved numerically by an electronic-computer and the potential function parameters $V_1=993$ cm^{-1}, $V_2=636$ cm^{-1}, and $V_3=44$ cm^{-1} are chosen to fit the internal-rotation energy-level scheme. The *trans* and *cis* potential barrier heights are 386 and 2460 cm^{-1}, respectively, and the potential-function minima are located 111.5° from the *cis* configuration. Diagonalization of the matrix of the complete Hamiltonian to second order by the use of perturbation theory is sufficient to account for the observed Q-branch shapes in the far infrared region.

Two microwave frequencies observed by Massey and Bianco at 22 054.5 and 27 639.6 Mc/sec are identified from their Stark effects as the first excited-state transitions $J, K, n, \tau=8, 6, 1, 1\rightarrow 7, 5, 1, 3$ and $J, K, n, \tau=8, 5, 1, 3\rightarrow 9, 6, 1, 1$, respectively, where the internal-rotation quantum number $n=1$ denotes the first excited torsional state and where τ denotes *trans* symmetric ($\tau=1$ and 2) or antisymmetric ($\tau=3$ and 4) states. The form of the dipole moment operator is assumed to be $\mu_0\cos(x/2)$ and μ_0 is found to be 3.15 D in agreement with the value obtained from the torsional ground-state transitions.

Two $J=0$ microwave series observed by Massey, Beard, and Jen in a mixed sample of the deuterated species D_2O_2 and HOOD give confirmation of the potential function determined from the H_2O_2 analysis. The $K=4\rightarrow 5$ series is identified as the D_2O_2 first excited torsional state transition $n=1\rightarrow 1$, $\tau=4\rightarrow 2$. The $K=0\rightarrow 1$ series is identified as the HOOD torsional ground-state transition $n=0\rightarrow 0$, $\tau=4\rightarrow 2$. Only very small changes in the *trans* barrier height are necessary to fit the constant terms of these series exactly. These changes, which are expected to arise from vibration–internal rotation interactions, show a reasonable progression from H_2O_2 to D_2O_2: $V(trans, \mathrm{HOOH})=386$ cm^{-1}, $V(trans, \mathrm{HOOD})=381$ cm^{-1} and $V(trans, \mathrm{DOOD})=378$ cm^{-1}.

I. INTRODUCTION

HYDROGEN peroxide is the simplest molecule having an internal-rotation motion. As shown in Fig. 1 the upper OH bar rotates relative to the lower OH bar subject to a hindering potential energy function $V(x)$, where x is the dihedral angle defining the relative position of the two OH bars. The problem attacked in this paper is the quantitative determination of the hindering potential function $V(x)$. It is found that a three-parameter potential is sufficient to account for the observed spectra. The three parameters are the height of the *trans* barrier V (*trans*), the height of the *cis* barrier V (*cis*), and the angle x_0 giving the position of the potential function minima. These numbers are determined by analysis of the far-infrared spectra of the vapor.

Hindered internal-rotation effects are observed in all regions of the hydrogen peroxide vapor spectrum. However, the hindering potential constants are such that the hindered rotation bands occur in the far infrared. Portions of these bands have been observed by Giguere and his co-workers,[1,2] but their prism resolution made it difficult to determine the band centers.

The microwave data of Massey *et al.*[3,4] give information about one internal-rotation energy splitting, but one splitting is insufficient to determine the three parameter potential function. Hirota[5] attempted the calculation of the barrier heights through investigation of the vibration–hindered-rotation interaction effects in the near-infrared spectra. Redington, Olson, and

* This research was supported in part by the Office of Naval Research and the Air Force Cambridge Research Laboratory.

† National Science Foundation Fellow, 1959–1962. Present address: Department of Physics, Florida State University, Tallahassee, Florida.

‡ Corning Glass Works Foundation Fellow, 1962–1963. Present address: CERN, Geneva 23, Switzerland.

[1] O. Bain and P. A. Giguere, Can. J. Chem. **33**, 527 (1955).
[2] D. Chin and P. A. Giguere, J. Chem. Phys. **34**, 690 (1961).
[3] J. T. Massey and D. R. Bianco, J. Chem. Phys. **22**, 442 (1954).
[4] J. T. Massey and R. W. Hart, J. Chem. Phys. **23**, 942 (1955).
[5] E. Hirota, J. Chem. Phys. **28**, 839 (1958).

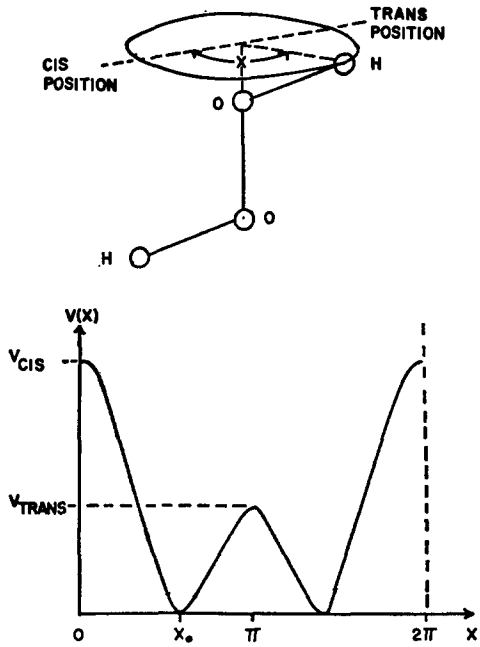

FIG. 1. The structure and hindering potential of H_2O_2.

Cross[6] made a high-resolution study of a vibrational band at 2650 cm^{-1}. Through an analysis of this band based upon a slightly asymmetric-top model with uncoupled internal and over-all rotations they obtained accurate ground-state rotational constants. In addition, they determined the internal-rotation ground-state splitting using their rotational constants and the microwave data of Massey, but they were unable to completely determine the potential function.

Presented in this paper are the results of a 0.3-cm^{-1} resolution study of the vapor absorption of hydrogen peroxide between 15 and 700 cm^{-1}. The present investigation contains a theory of internal rotation in the molecule in which the internal-rotation–over-all rotation interactions are retained. The analysis of the far infrared spectra using this theory yields the values $V(trans)=386$ cm^{-1}, $V(cis)=2460$ cm^{-1}, and $x_0=111.5°$ for the hindering potential parameters. Further, the origins of two previously unidentified microwave lines of the H_2O_2 vapor spectrum and two $\Delta J=0$ microwave series of the deuterated species spectrum are explained. A study of the microwave Stark effect leads to a quantitive expression for the electric-dipole-moment function of the molecule.

The paper is divided into five main sections. Section II describes the apparatus and experimental techniques used to obtain the far infrared spectra. The theory of internal rotation in the molecule is developed in Sec. III. In Sec. IV the far-infrared spectra are presented in detail and the theory of Sec. III is applied to these spectra to determine the hindering potential and the internal-rotation energy-level structure. Sections V and VI discuss the microwave spectra of H_2O_2 and the microwave spectra of the deuterated species HOOD and D_2O_2, respectively.

II. EXPERIMENT

The present data were taken using a multiple-reflection cell, 40-cm long, of the White type, in conjunction with a modified version of the vacuum grating spectrometer built by Randall and Firestone.[7] The optical path of this instrument is shown in Fig. 2. The radiation sources are a 400-W high-pressure mercury lamp for the region from 15 to 100 cm^{-1} and an electrically heated platinum strip, coated to increase its emissivity, for the region from 100 to 700 cm^{-1}. G_1, G_2, and G_3 are small gratings designed to remove higher-order radiation by dispersing it out of the beam. Spectral impurities using these gratings and a glass chopper are less than a few percent even when operating in the blaze of the main grating, G. The radiation is condensed on the Golay cell detector by means of a brass cone.

Water-vapor absorption due to decomposition of the hydrogen peroxide vapor within the cell is suppressed by (1) constructing the absorption cell of aluminum and glass fitting it with polyethylene windows to keep the decomposition rate at a minimum and (2) removing the decomposition products by pumping slowly on the cell which was open to a liquid reservoir of hydrogen peroxide maintained at about 25°C. This procedure reduces the water absorption to the point where only a few of the strongest water lines are visible in the spectrum.

The H_2O_2 sample as obtained from the Buffalo Electrochemical Corporation was 98% pure. Absorption paths ranged from 4.8 m at 700 cm^{-1} to 1.6 m at 30 cm^{-1}.

All spectra were taken in first order using grating spacings ranging from 15 to 2400 line/in. and recording time constants ranging from 18 to 105 sec. Grating calibration was by means of absorption lines of HCN, H_2O, and CO. Estimated accuracies in reporting single sharp lines are ± 0.05 cm^{-1} between 700 and 400 cm^{-1} and ± 0.03 cm^{-1} between 400 and 15 cm^{-1}.

III. THEORY OF HINDERED ROTATION

A. Hamiltonian

In the hydrogen peroxide molecule the lowest vibrational fundamental frequency is the OO stretching vibration at approximately 900 cm^{-1}. The frequencies associated with internal-rotation transitions are much lower than this and hence, it is a good first approximation to assume no interaction between the vibrational and internal-rotation motions. For this reason, the molecule is represented by a semirigid model; the OH distances, the OO distance and the OOH angles are assumed fixed. The general coordinates of the problem are the Eulerian angles ψ, θ, ϕ describing the

[6] R. L. Redington, W. B. Olson, and P. C. Cross, J. Chem. Phys. 36, 1311 (1962).

[7] H. M. Randall and F. A. Firestone, Rev. Sci. Instr. 9, 404 (1938).

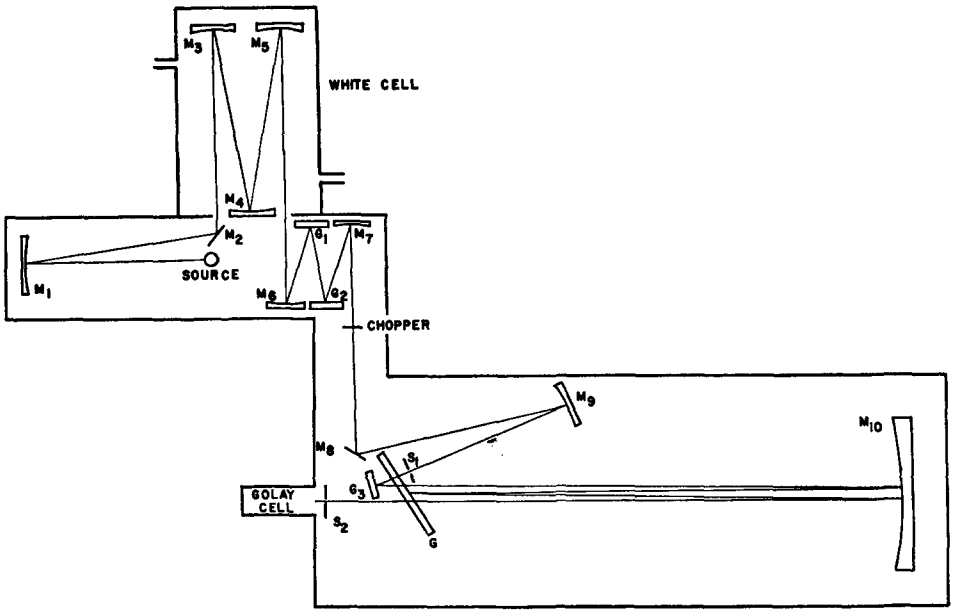

FIG. 2. Diagram of the spectrometer and fore optics.

orientation of the molecule in space and the internal angle x describing the relative orientation of the two OH bars.

The Eulerian angle ϕ and the internal angle x are defined by $\phi=\frac{1}{2}[\phi_1+\phi_2]$ and $x=\phi_1-\phi_2$ where ϕ_1 and ϕ_2 are the azimuthal angles of the upper and lower OH bars, respectively. The Eulerian angles ψ, θ, and ϕ describe the orientation of the center of mass molecule-fixed system x, y, z relative to the space-fixed coordinate system X, Y, Z while x is the instantaneous dihedral angle between the two OH bars (see Fig. 3).

The rotational kinetic energy of the molecule written in terms of the coordinates ψ, θ, ϕ, and x and their time derivatives is

$$2T=A(x)\omega_x^2+B(x)\omega_y^2+C(x)\omega_z^2+2D(x)\omega_y\omega_z +2F(x)\omega_x(\dot{x}/2)+G(x)(\dot{x}/2)^2, \quad (3.1)$$

where $\dot{x}$ is the time derivative of the internal angle x and where ω_x, ω_y, and ω_z are the components of the angular velocity of the molecule-fixed coordinate system along the molecule-fixed axes x, y, and z. The inertial parameters $A(x)\cdots G(x)$ are functions of the internal angle x as well as functions of the structural distances and angles of the molecule. The form and magnitude of these inertial parameters are given in Appendix I.

The classical Hamiltonian for the semirigid model of the hydrogen peroxide molecule is therefore

$$H=\frac{1}{2}\frac{G}{AG-F^2}P_x^2+\frac{1}{2}\frac{C}{BC-D^2}P_y^2 +\frac{1}{2}\frac{B}{BC-D^2}P_z^2+\frac{-D}{BC-D^2}P_yP_z +\frac{-2F}{AG-F^2}p_xP_x+\frac{1}{2}\frac{4A}{AG-F^2}p_x^2+V(x), \quad (3.2)$$

where

$$p_x=\partial T/\partial\dot{x}, \qquad P_i=\partial T/\partial\omega_i, \qquad i=1, 2, 3.$$

It can be shown that the quantities P_x, P_y, P_z represent the components of the total angular momentum of the molecule along the molecule-fixed axes x, y, z. P_x, P_y, and P_z are given in terms of the canonical momenta and coordinates p_ψ, p_θ, p_ϕ, ψ, θ, ϕ by the usual formulas. The momentum p_x is the canonical variable conjugate to the internal angle coordinate x. If the classical components P_x, P_y, P_z, and p_x are replaced by their quantum mechanical operators, the operators obey the commutation relations

$$[P_i, P_j]=-i\hbar P_k, \qquad [P_i, p_x]=0, \qquad [P_i, x]=0.$$

The quantity $V(x)$ is the internal rotation potential energy.

The interaction between the internal rotation and the over-all rotation of the molecule appears in two ways in the terms of the Hamiltonian (3.2). First, the inertial parameters are still functions of the internal angle x and second, the third row of the Hamiltonian contains the interaction term p_xP_x. The x dependence of the inertial parameters is a characteristic of the problem, but does not lead to strong interaction between internal and over-all rotations since it does not give rise to large matrix elements off-diagonal in the internal-rotation

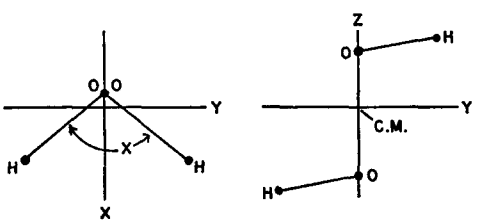

FIG. 3. The internal angle x.

quantum numbers. The momentum cross term p_xP_x, however, gives rise to matrix elements off-diagonal in the internal-rotation quantum numbers which may be, especially for large values of the barrier heights, of the same order of magnitude as internal-rotation energy differences and hence, difficult to account for by perturbation theory. For this reason, the p_xP_x term is removed by a contact transformation of the Hamiltonian similar to that used by Hecht and Dennison.[8] For the hydrogen peroxide molecule the form of the transformation is

$$p_x=p_x'-k(x)P_x', \qquad x=x',$$

$$\begin{pmatrix} P_x \\ P_y \\ P_z \end{pmatrix}=\begin{pmatrix} 1 & 0 & 0 \\ 0 & \cos u(x) & \sin u(x) \\ 0 & -\sin u(x) & \cos u(x) \end{pmatrix}\begin{pmatrix} P_x' \\ P_y' \\ P_z' \end{pmatrix}, \quad (3.3)$$

where $k(x)$ and $u(x)$ are functions of the internal angle x. $k(x)$ is chosen so that the transformed Hamiltonian does not contain a momentum-interaction term $p_x'P_x'$. $u(x)$ is chosen so that the proper commutation relations hold for the transformed components:

$$[P_i', P_j']=-i\hbar P_k', \qquad [P_i', p_x']=0, \qquad [P_i', x]=0.$$

These aims are accomplished with

$$k(x)=\partial u(x)/\partial x=-\tfrac{1}{2}[F(x)/A(x)],$$

where $F(x)$ and $A(x)$ are the inertial parameters of Eq. (3.1) given in Appendix I. The transformed Hamiltonian is[9]

$$H=\beta(x)P'^2+\nu(x)P_z'^2+\gamma(x)[P_x'^2-P_y'^2]$$
$$+\delta(x)[P_y'P_z'+P_z'P_y']+\alpha(x)p_x'^2+V(x), \quad (3.4)$$

where $P'^2=P_x'^2+P_y'^2+P_z'^2$. In the Hamiltonian (3.4) the interaction between the internal and over-all rotations appears only because the inertial coefficients of P_x', P_y', and P_z' are functions of the internal angle x. The momentum-interaction term p_xP_x is not present.

Because the hydrogen nuclear mass is small relative to the oxygen nuclear mass, the hydrogen peroxide molecule Hamiltonian will be that of a nearly symmetric top plus an internal-rotation Hamiltonian. For the same reason, the inertial coefficients of P_x', P_y', P_z', and p_x' will be "weak" functions of the internal angle x which can be expanded in rapidly convergent series of trigonometric functions of x. The Fourier expansion of these inertial coefficients is

$$\beta(x)=\beta_0+\beta_1\cos x+\beta_2\cos 2x+\cdots,$$
$$\nu(x)=\nu_0+\nu_1\cos x+\nu_2\cos 2x+\cdots,$$
$$\gamma(x)=\gamma_0+\gamma_1\cos x+\gamma_2\cos 2x+\cdots,$$
$$\alpha(x)=\alpha_0+\alpha_1\cos x+\alpha_2\cos 2x+\cdots,$$
$$\delta(x)=\delta_1\sin^{3}\tfrac{1}{2}x+\cdots. \quad (3.5)$$

The constants β_i, ν_i, γ_i, α_i, and δ_1 are functions of the fixed OO and OH distances and the fixed OOH angles. For the values: OO distance = 1.475 Å, OH distance = 0.950 Å and OOH angle = 94.8° (see Ref. 6) these constants are, in wavenumbers,

$$\beta(x)=0.859\ \text{cm}^{-1}+0.00247\cos x+0.000842\cos 2x+\cdots,$$
$$\nu(x)=9.158-0.1031\cos x+0.00784\cos 2x+\cdots,$$
$$\gamma(x)=0.000487+0.0367\cos x+0.000202\cos 2x+\cdots,$$
$$\alpha(x)=39.945+0.248\cos x+0.0433\cos 2x+\cdots,$$
$$\delta(x)=0.0902\sin^{3}\tfrac{1}{2}x+\cdots. \quad (3.6)$$

These expansions show that in lowest order the Hamiltonian (3.4) separates into a rigid symmetric-top Hamiltonian

$$H_{\text{symmetric top}}=\beta_0P'^2+\nu_0P_z'^2 \quad (3.7)$$

plus an internal-rotation Hamiltonian

$$H_{\text{internal rotation}}=\alpha(x)p_x'^2+V(x). \quad (3.8)$$

The solutions of the symmetric-top wave equation are well known. The study of the internal-rotation Hamiltonian is undertaken in the next section. The remaining internal-rotation–over-all-rotation interaction terms are small and their effects on the energy levels are calculated by the use of perturbation theory. It should be noted, however, that the asymmetric coefficient $\gamma(x)$, though small, is strongly x-dependent so that the small asymmetry effects cannot be expected to be given by rigid asymmetric-rotator theory.

B. Internal Rotation Problem

Penney and Sutherland[10] proposed that the two dominant effects determining the hindering potential energy are (1) the interaction between the two nonbonded pairs of p electrons associated with the oxygen atoms and (2) the interaction between the dipole moments associated with the OH groups. The interaction of the two nonbonded electron pairs has a periodicity of π and its dominant term is expected to be of the form $V_2\cos 2x$ with minima at $x=\pi/2$ and $x=3\pi/2$ halfway between the *cis* ($x=0$) and *trans* ($x=\pi$) positions. The interaction of the dipoles associated with the two OH groups has a periodicity of 2π with a dominant term of the form $V_1\cos x$ which gives

[8] K. T. Hecht and D. M. Dennison, J. Chem. Phys. **26**, 31 (1957).

[9] The term $\alpha(x)p_x'^2$ is not in correct quantum mechanical form because the internal angle coordinate x does not commute with the operator p_x'. The term is written in this form for brevity and is, of course, symmetrized before calculations are made.

[10] W. G. Penney and G. B. B. M. Sutherland, J. Chem. Phys. **2**, 492 (1934).

preference to the *trans* position. The precise shape of the barriers may be determined by smaller $\cos 3x$, $\cos 4x$, $\cdots$ terms.

In order to have three disposable parameters so that $V(cis)$, $V(trans)$, and x_0 can be varied independently, the following form is chosen for the hindering potential function

$$V(x) = V_1 \cos x + V_2 \cos 2x + V_3 \cos 3x, \qquad (3.9)$$

where $V_3 \cos 3x$ must be expected to be a small correction term. The expressions relating V_1, V_2, and V_3 to $V(trans)$, $V(cis)$, and x_0 are given in Appendix II.

Since a hindering potential function of arbitrary shape could be expanded in a Fourier cosine series, the potential function (3.9), which contains the first three terms of such a series, could be the starting point of the investigation of the far-infrared spectrum even without any knowledge of the electronic structure of the molecule. In this investigation, the final justification of the form (3.9) is its success in explaining the far-infrared and microwave spectra of hydrogen peroxide vapor.

The internal-rotation wave equation is now the Mathieu-type equation

$$[\alpha(x) p_x'^2 + V_1 \cos x + V_2 \cos 2x + V_3 \cos 3x] M(x) = EM(x) \qquad (3.10)$$

with eigenfunctions of the form[11] $M(x) = P(x) \exp(i\sigma x)$ with $P(x+2\pi) = P(x)$. Therefore the total zeroth-order molecular wavefunctions are

$$u = (1/2\pi) e^{iK\phi'} e^{iM\psi'} \Theta_{JKM}(\theta') [e^{i\sigma x} P(x)], \qquad (3.11)$$

where the $(1/2\pi) \exp(iK\phi') \exp(iM\psi') \Theta_{JKM}(\theta')$ are the symmetric-top wavefunctions $\Psi_{JKM}(\psi, \theta, \phi)$ with J, K, and M integers. σ is determined by the boundary conditions on ϕ' and x. If either of the two OH groups is rotated through an integral multiple of 2π the configuration of the molecule is unchanged. Hence, u must be invariant under the transformations $\phi_1 \rightarrow \phi_1 + 2\pi n_1$, $\phi_2 \rightarrow \phi_2 + 2\pi n_2$, where n_1 and n_2 are arbitrary integers. In terms of ϕ and x these transformations are $\phi \rightarrow \phi + (n_1+n_2)\pi$, $x \rightarrow x + (n_1 - n_2) 2\pi$. In terms of the coordinates ϕ' and $x' = x$ these transformations again have the form[8] $\phi' \rightarrow \phi' + (n_1+n_2)\pi$, $x' \rightarrow x' + (n_1 - n_2) 2\pi$. The requirement that u be invariant under these transformations[12] leads to $\sigma = -K/2$ and hence to

$$M(x) = \exp[-i(K/2)x] P(x) \qquad (3.12)$$

and $M(x+2\pi) = (-1)^K M(x)$.

Table I. Symmetry of the internal-rotation wavefunctions.

K value (even or odd)	Symmetry under σ_t	Symmetry under σ_c	τ Quantum number	Expansion of internal-rotation wavefunctions
e	s	s	1	$M_1(x) = \pi^{-1} \Sigma a(n) \cos nx$
o	s	a	2	$M_2(x) = \pi^{-1} \Sigma b(n) \sin(n+\frac{1}{2})x$
o	a	s	3	$M_3(x) = \pi^{-1} \Sigma c(n) \cos(n+\frac{1}{2})x$
e	a	a	4	$M_4(x) = \pi^{-1} \Sigma d(n) \sin nx$

[11] E. T. Whittaker and G. N. Watson, *Modern Analysis* (Cambridge University Press, New York, 1958), 4th ed., p. 412.

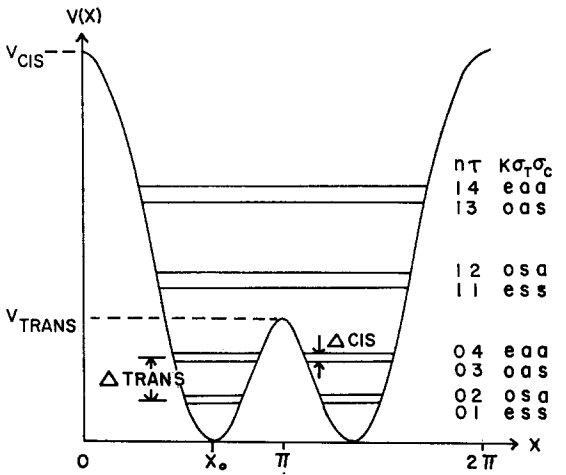

FIG. 4. The internal-rotation energy levels.

Since the internal-rotation wave equation is unchanged by reflection in either the *cis* or *trans* plane, that is, by the operations $x \rightarrow -x$ and $x \rightarrow 2\pi - x$, its solutions have four basic symmetries:

$$\sigma(cis) M(x) = M(-x) = \pm M(x),$$
$$\sigma(trans) M(x) = M(2\pi - x) = \pm M(x).$$

Therefore $\sigma(cis)\sigma(trans) M(x) = (-1)^K M(x)$ and it follows that internal-rotation levels have the same *cis* and *trans* symmetry when K is even and opposite *cis* and *trans* symmetry when K is odd. The four types of internal-rotation wavefunctions with their symmetries and associated K values are shown in Table I. An internal-rotation quantum number τ differentiates the four symmetry types. The appropriate Fourier series used to expand the $M_\tau(x)$ are also shown.

Figure 4 shows a hindering potential for H_2O_2 with $V(cis) > V(trans)$ and its associated energy levels of internal rotation. A second internal-rotation quantum number n is introduced. This principal quantum number orders the energy levels of a given symmetry τ: the first quartet of levels is $n=0$, $\tau = 1, 2, 3, 4$, the second quartet is $n=1$, $\tau = 1, 2, 3, 4$ and so on for higher values of n.

The energy splittings within a quartet are sensitive functions of the heights and widths of the *cis* and *trans* potential hills. In the limit in which $V(cis) \rightarrow \infty$ levels with $\tau = 1$ and 2 and the same n become degenerate; the same is true for levels with $\tau = 3$ and 4 and the same n. If, in addition, $V(trans) \rightarrow \infty$ all four levels of a given n become degenerate. The $\tau = (1, 2)$ and $(3, 4)$

[12] J. S. Koehler and D. M. Dennison, Phys. Rev. **57**, 1006 (1940).

splittings, $\Delta(cis)$, are thus associated with tunnelling through the *cis* barrier while the separation of the pair $\tau=(1,2)$ from the pair $\tau=(3,4)$, $\Delta(trans)$, is associated with tunneling through the *trans* barrier.

The numerical solution of the internal-rotation wave equation (3.10) was performed on the IBM 7090 computer at the Computing Center of the University of Michigan. The Hamiltonian matrices are formed using as basis functions, the orthonormal sets of Table I. The energy matrices are diagonalized by the application of a series of two by two rotations which successively eliminate the largest off-diagonal component.[13] The result is a set of internal-rotation eigenvalues, $E_{n\tau}$, and eigenvectors, $M_{n\tau}(x)$, which depend upon the input values of V_1, V_2, and V_3. In this way, a set V_1, V_2, V_3 is found which produces an internal-rotation energy level scheme that explains the far-infrared spectrum.

Matrix elements of the quantities $\cos x$, $\cos 2x$, $\sin^3(x/2)$, and $\cos(x/2)$ are also computed numerically for use in the perturbation-theory calculations.

C. Matrix Elements of the Hamiltonian

The eigenfunctions of the symmetric top, $\Psi_{JKM}(\psi,\theta,\phi)$, and the eigenfunctions of the internal-rotation Hamiltonian, $M_{n\tau}(x)$, are used to form the basis functions for the matrix of the complete Hamiltonian. Since the complete Hamiltonian [see Eqs. (3.4) and (3.5)] for the semirigid model of the hydrogen peroxide molecule is invariant under the symmetry operations C_{2x} and $\sigma(trans)$ use of the basis functions

$$\Psi_{J(K\pm)Mn\tau}=(1/\sqrt{2})[\Psi_{JKM}\pm\Psi_{J(-K)M}]M_{n\tau}$$
$$\Psi_{J0Mn\tau}=\Psi_{J0M}M_{n\tau} \tag{3.13}$$

will factor the energy matrix, for a given value of J, into four submatrices corresponding to the four possible symmetry types given in Table II. This choice of basis functions also removes the K degeneracy of the $K=\pm1$ states in zeroth approximation since the $K=\pm1$ states are connected by the $\gamma(x)[P_x'^2-P_y'^2]$ asymmetry term.

The matrix elements of the Hamiltonian (3.4), diagonal in the quantum number K, are

$$\begin{aligned}
H_{JK+n\tau}{}^{JK+n\tau}&=\beta_{n\tau}{}^{n\tau}J(J+1)+\nu_{n\tau}{}^{n\tau}K^2+E_{n\tau}, \qquad K\neq1,\\
H_{J(1\pm)n\tau}{}^{J(1\pm)n\tau}&=[\beta_{n\tau}{}^{n\tau}\pm\tfrac{1}{2}\gamma_{n\tau}{}^{n\tau}]J(J+1)+\nu_{n\tau}{}^{n\tau}+E_{n\tau},\\
H_{JK+n\tau}{}^{JK+n'\tau}&=\beta_{n\tau}{}^{n'\tau}J(J+1)+\nu_{n\tau}{}^{n'\tau}K^2, \qquad n'\neq n,\ K\neq1,\\
H_{J(1\pm)n\tau}{}^{J(1\pm)n'\tau}&=[\beta_{n\tau}{}^{n'\tau}\pm\tfrac{1}{2}\gamma_{n\tau}{}^{n'\tau}]J(J+1)+\nu_{n\tau}{}^{n'\tau}, \qquad n'\neq n.
\end{aligned} \tag{3.14}$$

The matrix elements of the Hamiltonian (3.4), off-diagonal in the quantum number K, are

$$\begin{aligned}
H_{JK+n\tau}{}^{J(K+1)+n'\tau'}&=-\delta_{n\tau}{}^{n'\tau'}i\tfrac{1}{2}(2K+1)[(J-K)(J+K+1)]^{\frac{1}{2}}, \qquad \tau'\neq\tau,\ K\geq1,\\
H_{J0n\tau}{}^{J1+n'\tau'}&=-\delta_{n\tau}{}^{n'\tau'}i[\tfrac{1}{2}J(J+1)]^{\frac{1}{2}}, \qquad \tau'\neq\tau,\\
H_{JK+n\tau}{}^{J(K+2)+n'\tau'}&=\gamma_{n\tau}{}^{n'\tau'}\tfrac{1}{2}[(J-K-1)(J-K)(J+K+1)(J+K+2)]^{\frac{1}{2}}, \qquad K\geq1,\\
H_{J0n\tau}{}^{J2+n'\tau'}&=\gamma_{n\tau}{}^{n'\tau'}\tfrac{1}{2}[(J-1)(J)(J+1)(J+2)]^{\frac{1}{2}}.
\end{aligned} \tag{3.15}$$

The internal-rotation matrix elements of $\beta(x)$, $\nu(x)$, $\gamma(x)$, and $\delta(x)$ used in the above expressions are integrals of the form

$$\nu_{n\tau}{}^{n'\tau'}=\int M_{n\tau}{}^*(x)\nu(x)M_{n'\tau'}(x)dx.$$

The matrix elements between the K^- states are identical to those given above for the K^+ states with the exception that the $K=0$ state is not connected to the K^- states (see Table II.) Since the off-diagonal matrix elements are small the energy levels of the semirigid model of the molecule can be calculated to an accuracy of several hundredths of a wavenumber by the use of second-order perturbation theory.

The zeroth-order selection rules for the hydrogen peroxide molecule follow from the symmetry of the molecular wavefunctions given in Table II. The quantum number K must change by 1 in a dipole transition because the electric dipole moment is perpendicular to the molecule-fixed z' axis. As usual, the quantum number J has the dipole selection rules $\Delta J=0,\pm1$. The projection of the dipole moment, $\mu(x)$, on the

TABLE II. Symmetry of the basis functions.

Type of basis functions		Symmetry under C_{2x}	Symmetry under $\sigma(trans)$
Ψ_{JK+} and Ψ_{JO},	$\tau=1,2$	$(-1)^{J}$[a]	$+1$
Ψ_{JK-} ,	$\tau=1,2$	$-(-1)^{J}$	$+1$
Ψ_{JK+} and Ψ_{JO},	$\tau=3,4$	$(-1)^{J}$	-1
Ψ_{JK-} ,	$\tau=3,4$	$-(-1)^{J}$	-1

[13] The actual internal rotation energy matrices are infinite, but the lower eigenvalues ($n=0,1,2,3$) are virtually unaffected by states whose diagonal matrix elements are large. Therefore, diagonalization of a finite energy matrix gives an extremely good approximation to the lower eigenvalues. For example, the differences between the lower eigenvalues of an 18×18 energy matrix and the lower eigenvalues of a 30×30 energy matrix are less than 0.0002 cm^{-1} when both matrices are diagonalized by the computer.

[a] The symmetry under C_{2x} follows from the well-known property of the symmetric-top eigenfunctions: $C_{2x}\Psi_{JK}=(-1)^{J}\Psi_{J-K}$.

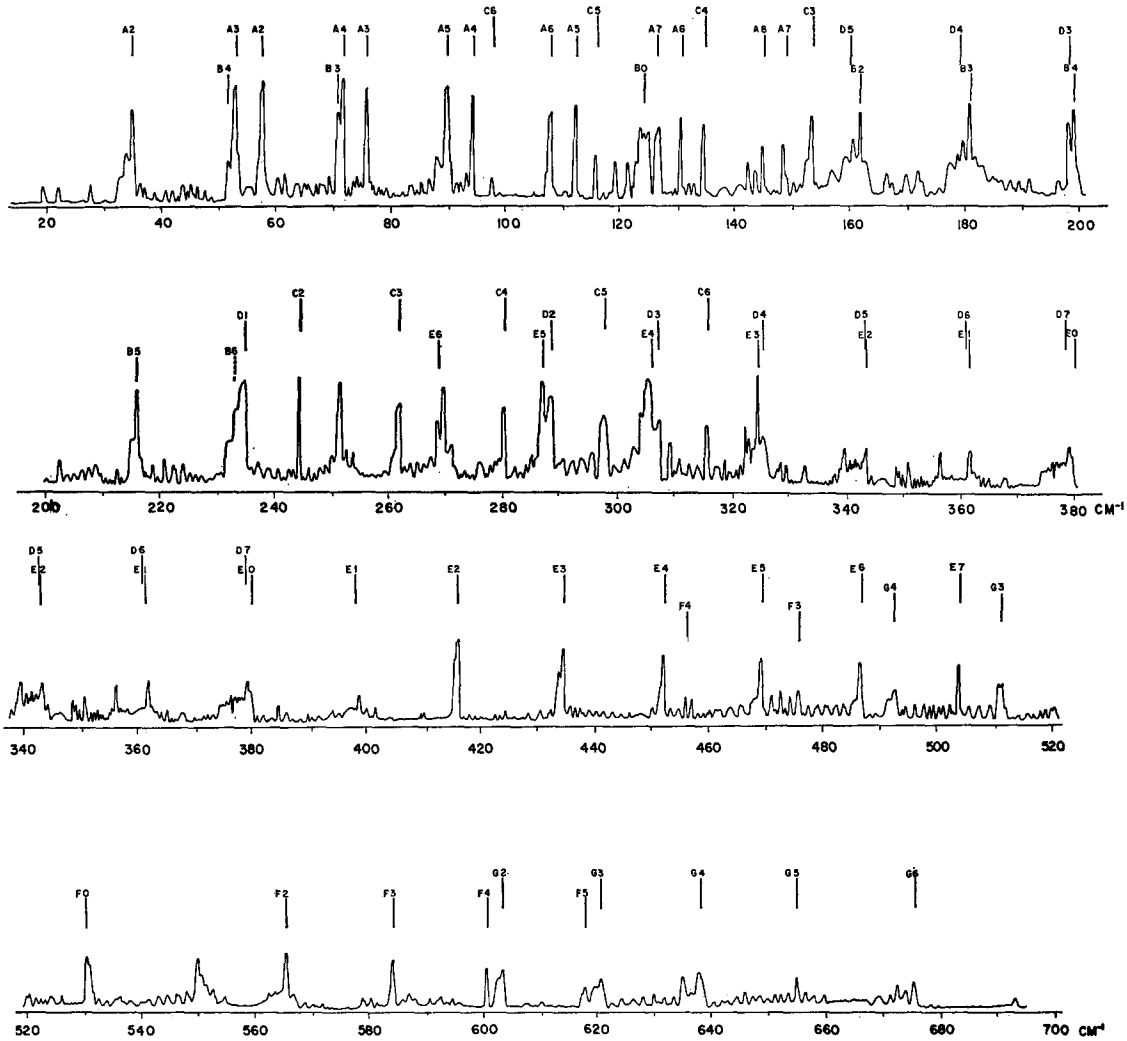

FIG. 5. The absorption spectrum of H_2O_2 vapor from 15 to 700 cm^{-1}.

space-fixed Z axis is $\mu_0 \cos(x/2) \cos(x', Z)$ since the dipole moment is along x' in the molecule-fixed axis system.[14] Under the symmetry operations C_{2x} and $\sigma(trans)$ the behavior of $\cos(x/2)$ and $\cos(x', Z)$ is

$$\sigma(trans) \cos(x/2) = -\cos(x/2),$$
$$C_{2x} \cos(x', Z) = +\cos(x', Z).$$

Therefore, states of opposite *trans* symmetry are connected. If $\Delta J=0$, the connections are $K+\leftrightarrow K'+$ and $K-\leftrightarrow K'-$ and if $\Delta J=\pm 1$, the connection is $K+\leftrightarrow K'-$. The rules are summarized in Table III.

IV. FAR-INFRARED SPECTRA AND THE DETERMINATION OF THE HINDERING POTENTIAL

A. Results

The observed far-infrared absorption of hydrogen peroxide vapor is plotted versus frequency in Fig. 5. The positions of the principal absorption lines, the percent absorption at the line peak, and the half-width of the lines including the instrumental half-width are listed in Table IV. Because of the uncertainty of the H_2O_2 vapor pressure in the absorption cell, the relative intensities of the lines are only approximate.

The anticipated perpendicular character of the hindered-rotation bands is evident and several band centers, particularly those at 11.43, 198.7, and 370.7 cm^{-1}, can be found readily from a perpendicular band analysis. The remaining band centers present greater

TABLE III. Selection rules for hydrogen peroxide.

$\Delta J=0$ transitions	$\Delta J=\pm 1$ transitions
$K+\rightarrow K'+$	$K+\rightarrow K'-$
$K-\rightarrow K'-$ with $\Delta K=\pm 1$	$K-\rightarrow K'+$ with $\Delta K=\pm 1$
$n\rightarrow n'$	$n\rightarrow n'$
$\tau=1\leftrightarrow 3$ or $\tau=2\leftrightarrow 4$	$\tau=1\leftrightarrow 3$ or $\tau=2\leftrightarrow 4$

[14] Experimental justification for the form $\mu(x)=\mu_0 \cos(x/2)$, where μ_0 is a constant, is presented in the H_2O_2 microwave discussion, Sec. V.

TABLE IV. Frequencies of the principal absorption lines of H_2O_2 vapor.

Frequency (cm^{-1})	Percent absorption	Half-width (cm^{-1})	Frequency (cm^{-1})	Percent absorption	Half-width (cm^{-1})	Frequency (cm^{-1})	Percent absorption	Half-width (cm^{-1})
34.56	45	0.4	161.98	43	0.6	361.94	27	...
51.78	20	...	179.14	38	0.7	379.44	27	...
52.94	55	0.9	180.11	52	0.7	399.01	20	...
57.38	60	0.5	196.75	35	1.0	416.11	42	1.0
70.49	40	...	197.99	45	1.0	434.06	30	1.3
71.36	62	0.7	215.74	45	0.5	451.70	23	1.0
75.67	50	0.5	234.2	50	1.9	456.21	26	0.6
89.69	55	0.8	244.00	55	0.5	469.20	45	1.2
94.08	45	0.5	251.34	50	1.1	475.40	25	0.7
97.57	15	0.4	261.97	40	1.0	486.61	33	1.2
107.90	38	0.9	267.97	36	0.9	492.5	17	2.0
112.27	42	0.4	269.42	47	1.1	503.85	33	0.8
115.91	24	0.6	279.96	38	0.7	511.3	17	1.9
120.10	20	0.8	286.93	48	1.4	530.4	21	1.3
121.81	20	0.4	288.42	43	1.3	549.4	24	1.2
124.5	30	2.0	297.65	34	1.2	566.41	30	0.7
126.76	30	0.7	305.4	50	2.0	583.80	30	0.7
130.33	40	0.4	307.10	32	0.9	601.01	22	0.7
134.37	35	0.5	308.96	20	0.5	603.0	20	1.6
142.19	20	0.4	315.42	30	0.9	617.8	12	0.9
143.42	17	0.6	322.44	30	...	620.6	17	2.0
144.55	28	0.5	324.46	52	0.6	634.9	14	0.7
148.37	26	0.7	339.77	23	...	638.3	17	0.9
152.92	40	0.6	343.31	25	...	655.5	12	0.9
160.71	31	0.8	357.27	26	...	674.5	12	0.6

difficulty in their determination, either because the number of Q branches observed for a given band is small, or because the Q-branch widths exhibit peculiarities.

Seven hindered-rotation bands have been identified. The frequencies of their band centers are listed in Table V along with the internal-rotation level assignments for the transition. Since the same internal-rotation level is usually involved in more than one band, the band centers are estimated to be accurate to ± 0.05 cm^{-1} except for the 11.43 cm^{-1} band which is determined to ± 0.01 cm^{-1} from the microwave data. These seven bands account for nearly all of the stronger absorption lines of the spectrum. The justification for these assignments is presented later in this section.

No alternation of the Q-branch spacings in any band is observed. This indicates a high *cis* barrier with negligible tunneling through it. The *cis* barrier splittings ($E_{n2}-E_{n1}$ and $E_{n4}-E_{n3}$) are estimated to be less than 0.002 cm^{-1} for the lower torsional states ($n=0, 1, 2$), so that for a given value of n the $\tau=1$ and 2 levels and similarly the $\tau=3$ and 4 levels can be considered degenerate for purposes of calculation.

TABLE V. Observed band frequencies and band assignments.

	Band frequency	Internal rotation transition $n\tau \rightarrow n'\tau'$
A	11.43 cm^{-1}	01↔03 and 02↔04
B	116.51	11→13 and 12→14
C	198.57	13→21 and 14→22
D	242.76	03→11 and 04→12
E	370.70	01→13 and 02→14
F	521.68	11→23 and 12→24
G	557.84	03→21 and 04→22

The hindering potential function required to fit these internal transitions is dependent on the choice of the OO bond distance, $r(OO)$, the OH bond distance, $r(OH)$, and the OOH angle. It is necessary to fit both the observed internal-rotation energy levels and the observed matrix elements of $\beta(x)$, $\nu(x)$, $\gamma(x)$, and $\delta(x)$ (which determine the structure of the bands) with the six quantities V_1, V_2, V_3; $r(OO)$, $r(OH)$, and the OOH angle.

The hindering potential and the matrix elements of $\beta(x)$, $\nu(x)$, $\gamma(x)$, and $\delta(x)$ are calculated using the structural parameters of Redington, Olson, and Cross: $r(OH)=0.950\pm0.005$ Å, $r(OO)=1.475\pm0.004$ Å and the OOH angle $=94.8\pm2.0°$. The present investigation confirms these values for the structural parameters well within the error limits quoted. Table VI lists some internal-rotation matrix elements for $n=0, 1, 2$.

TABLE VI. Some calculated internal rotation matrix elements for $n=0, 1, 2$.

$n\tau$	$\beta_{n\tau}{}^{n\tau}$	$\nu_{n\tau}{}^{n\tau}$	$\gamma_{n\tau}{}^{n\tau}$
01, 02	0.8574 cm^{-1}	9.204	−0.0168
03, 04	0.8574	9.198	−0.0148
11, 12	0.8575	9.226	−0.0228
13, 14	0.8576	9.199	−0.0148
21, 22	0.8578	9.196	−0.0136
23, 24	0.8580	9.186	−0.0100

$\delta_{01}{}^{02}=-0.058$ cm^{-1}	$\gamma_{01}{}^{11}=-0.010$	$\gamma_{13}{}^{23}=0.013$
$\delta_{03}{}^{04}=-0.055$	$\gamma_{02}{}^{12}=0.010$	$\gamma_{14}{}^{24}=0.013$
$\delta_{11}{}^{12}=-0.069$	$\gamma_{03}{}^{13}=0.010$	$\gamma_{21}{}^{31}=-0.014$
$\delta_{13}{}^{14}=-0.056$	$\gamma_{04}{}^{14}=0.010$	$\gamma_{22}{}^{32}=0.014$
$\delta_{21}{}^{22}=-0.055$	$\gamma_{11}{}^{21}=-0.012$	$\gamma_{23}{}^{33}=0.015$
$\delta_{23}{}^{24}=-0.050$	$\gamma_{12}{}^{22}=-0.012$	$\gamma_{24}{}^{34}=-0.015$

The hindering potential and internal-rotation energy level scheme are shown in Fig. 6. The letters labeling the internal-rotation transitions corresponds to the letters of Fig. 5 and Table V. The three-term potential function $V(x)\,(\mathrm{cm}^{-1})=993\cos x+636\cos 2x+44\cos 3x$ is sufficient to fit the six experimental levels well. The hindering potential may also be characterized by

$$V(trans)=386\pm 4\ \mathrm{cm}^{-1},$$
$$V(cis)=2460\pm 25\ \mathrm{cm}^{-1},$$
$$x_0=111.5\pm 0.5^\circ, \qquad (4.1)$$

where the uncertainties are estimated on the basis of the semirigid model of this investigation. The true uncertainties are larger than those given above because the semirigid model of hydrogen peroxide neglects the vibration–internal-rotation interactions. This hindering potential function is therefore an effective potential function and the parameters (4.1) represent average values for the vibrational ground state.

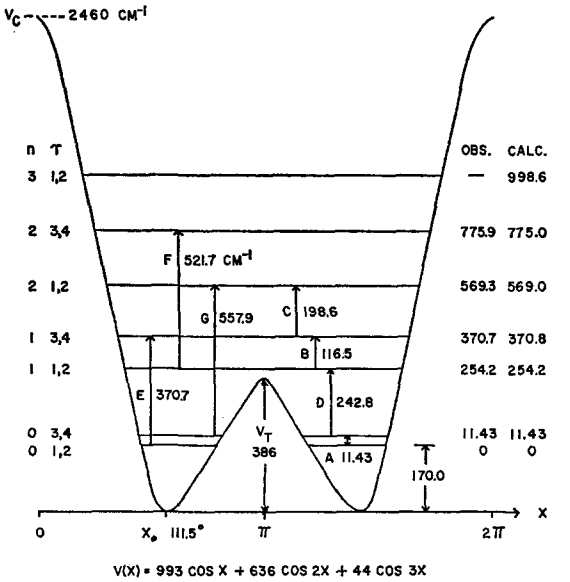

FIG. 6. The hindering potential and internal-rotation energy levels of H_2O_2.

B. Discussion of the Hindered Rotation Bands

The large amount of band overlap and the moderate resolution available combine to prevent any analysis of the P and R branch structure of the Q subbands. As evidenced by the absorption widths, very few individual P and R branch lines are resolved.

For purposes of analysis the peak absorption frequencies of the Q branches are taken as approximate Q-subband heads. In the symmetric top approximation the frequencies of the Q-subband heads in the $n\tau\rightarrow n'\tau'$ hindered rotation band are

$$^RQ_K(0)=\nu_{n'\tau'}{}^{n'\tau'}(K+1)^2-\nu_{n\tau}{}^{n\tau}K^2 +E_{n'\tau'}-E_{n\tau}-D_K[(K+1)^4-K^4],$$
$$^PQ_K(0)=\nu_{n'\tau'}{}^{n'\tau'}(K-1)^2-\nu_{n\tau}{}^{n\tau}K^2 +E_{n'\tau'}-E_{n\tau}-D_K[(K-1)^4-K^4], \qquad (4.2)$$

where a distortion coefficient D_K has been added to correct for vibration–over-all-rotation interactions.

11.43-cm^{-1} Band

The two series of Q branches labeled A in Fig. 5 beginning near the low-frequency end of the spectrum and extending to about 150 cm^{-1} with decreasing intensity arise from the internal-rotation transitions $n\tau=01\leftrightarrow 03$ and $02\leftrightarrow 04$ with band center at 11.43 cm^{-1}. The absence of any other strong series of Q branches beginning at low frequency is evidence that there are no lower-energy hindered-rotation states with a consequent smaller splitting. Series A are analyzed using combination sums and the value of D_K is found to be 4.4×10^{-4} cm^{-1}.

Table VII shows observed Q-branch frequencies and those calculated using a ground-state splitting $E_{04}-E_{02}=11.43$ cm^{-1}. (This splitting has been chosen for the most accurate fit to the microwave data; see Sec. *V*.) The only significant disagreement occurs for the transition $K=7\rightarrow 8$, $n\tau=03\rightarrow 01$. This discrepancy is explained by the second-order perturbation correction to the final state of the transition, $JKn\tau=J, 8, 0, 1$. The $J, K, n, \tau=J, 8, 0, 1$ energy level is found to be only 3.2 cm^{-1} above the $J, 6, 1, 1$ energy level to which it is connected by the $\gamma_{n\tau}{}^{n\tau}[P_x{}'^2-P_y{}'^2]$ term of the Hamiltonian. One result of this resonance is to shift the position of the Q branch about 0.5 cm^{-1} to higher frequency in agreement with the observed position.

The spectra showed little or no trace of absorption by Q branches involving $K=1$ for this band. Calculations based on the matrix elements listed in Table VI show that these Q branches should be several wavenumbers wide and thus lost in the background.

The six remaining hindered rotation bands have been analyzed in similar fashion using combination differences wherever possible. The average experimental values of $\nu_{n\tau}{}^{n\tau}$ for the $n=0$, 1, 2 levels are listed in Table VIII along with the value of D_K which was found to be consisted with all bands.

Table IX lists the observed and computed Q-branch frequencies for the remaining six hindered rotation bands. The computed positions are based upon the band centers of Table V and the rotational constants of Table VIII. Because of the Q-branch widths involved, deviations of less than 0.2 cm^{-1} are not significant.

In the following discussion, all calculations of the Q-branch shapes are based on the computed matrix elements of Table VI.

198.57-cm^{-1} Band

The 198.57-cm^{-1} band is the least overlapped. There is some unexplained alternation in the Q-branch widths on the R side of the band, but otherwise this band is well behaved. Calculations show that the four central

TABLE VII. Calculated and observed Q-branch frequencies of the internal rotation ground-state transitions (11.43 cm^{-1} band).

	$n\tau=01\rightarrow03$, $02\rightarrow04$		$n\tau=03\rightarrow01$, $04\rightarrow02$	
K	Calc.	Obs.	Calc.	Obs.
$0\rightarrow1$	20.63	...	−2.23	−2.23[a]
$1\rightarrow2$	39.03	...	16.17	...
$2\rightarrow3$	57.39	57.38	34.61	34.56
$3\rightarrow4$	75.71	75.67	53.00	52.94
$4\rightarrow5$	94.00	94.08	71.38	71.36
$5\rightarrow6$	112.20	112.27	89.71	89.69
$6\rightarrow7$	130.31	130.33	107.96	107.90
$7\rightarrow8$	148.42	148.37	126.24	126.76
$8\rightarrow9$	166.42	...	144.41	144.55

[a] Based on microwave data of Massey and Bianco.

Q branches should be sufficiently spread so as to be lost in the background.

370.70-cm^{-1} Band

The 370.70-cm^{-1} band has a clean R side, but several of the ^PQ branches are overlapped, especially $^PQ_4$, whose identification is uncertain. Spectra taken at 3.2-m path length show broad absorptions for the four central Q branches. After allowance for the calculated shapes of these Q branches, there is additional broad absorption on their low-frequency sides. A plot of the P and R structure of these Q subbands failed to disclose any accidental piling up. These additional broad absorptions are assigned to the 242.76 cm^{-1} band.

242.76-cm^{-1} Band

$^RQ_2$ and $^PQ_3$ for this band are identified and they have about the predicted width, but the Q branches for larger K values are all several wavenumbers wide, a result not predicted by the theory. The computed positions of the Q branches of this band are indicated in Fig. 5 to show that broad absorptions occur at the positions of the higher KQ branches. The frequency assignment of the band center has been made using the level positions determined from the other bands. Calculations of the shapes of the four central Q branches yields an interesting result for $^PQ_1$. Examination of the calculated matrix elements shows that the $n\tau=11$, 12 level (which is the upper level for the 242.76 cm^{-1} transition) has a $\gamma_{n\tau}{}^{n\tau}$ (or "asymmetry") approximately 40% larger than that for all other levels. As a result, the second order asymmetry correction to the $K=0$ level in the $n\tau=11$, 12 state is of sufficient magnitude to produce significant opposition to the large first-order $-(1/2)\gamma_{n\tau}{}^{n\tau}J(J+1)$ term which ordinarily spreads the $^PQ_1$ branch. The calculated J dependence of this branch is $^PQ_1(J)=233.56+7.2\times10^{-3}J(J+1)-6.1\times10^{-6}J^2(J+1)^2$. This calculated Q branch is plotted in Fig. 7 along with the observed absorption in this region. (Only transitions with nuclear spin weight 3 are shown.) The computed and observed absorptions agree well enough in width and position to assign the absorption to $^PQ_1$. This agreement, along with the well-behaved $^RQ_2$ and $^PQ_3$ branches, indicates that only the higher KQ branches in this band deviate markedly from the theoretical predictions.

TABLE VIII. Experimental values of $\nu_{n\tau}{}^{n\tau}$ for $n=0$, 1, 2.

$\nu_{01}{}^{01}=\nu_{02}{}^{02}=9.209\pm0.005$ cm^{-1}
$\nu_{03}{}^{03}=\nu_{04}{}^{04}=9.203\pm0.005$
$\nu_{11}{}^{11}=\nu_{12}{}^{12}=9.18\pm0.01$
$\nu_{13}{}^{13}=\nu_{14}{}^{14}=9.142\pm0.005$
$\nu_{21}{}^{21}=\nu_{22}{}^{22}=9.11\pm0.01$
$\nu_{23}{}^{23}=\nu_{24}{}^{24}=9.05\pm0.01$

$D_K=(4.4\pm1.0)\times10^{-4}$ cm^{-1} for all bands.

116.51-cm^{-1} Band

Although the appearance of the $^PQ_1$ branches of the 242.76-cm^{-1} band is satisfying both in the agreement with the theory and in the fact that an otherwise unexplained absorption is accounted for, the strongest proof for the assignment of that band comes from the identification of the 116.51-cm^{-1} band. Only two ^PQ branches are identifiable as this band suffers from a rapid decrease in the ^PQ-branch intensities as K in-

TABLE IX. Calculated and observed Q-branch frequencies for six hindered-rotation bands.

Q	370.70 band (E)		198.57 band (C)		116.51 band (B)		521.68 band (F)		557.84 band (G)		242.76 band (D)	
Branch	Calc.	Obs.	Calc.	Obs.	Calc.	Obs.	Calc.	Obs.	Calc.	Obs.	Calc.	Obs.
$^RQ_7$	503.80	503.85 cm^{-1}										
$^RQ_6$	486.64	486.61	315.47	315.42								
$^RQ_5$	469.30	469.20	297.77	297.65	215.78	215.74	617.94	617.80	655.54	655.5	342.94	b
$^RQ_4$	451.75	451.70	279.95	279.96	197.99	197.98	600.89	601.01	638.26	638.3	324.90	b
$^RQ_3$	434.01	434.06	261.99	261.97	180.06	180.11	583.83	583.80	620.74	620.6	306.76	b
$^RQ_2$	416.11	416.11	243.98	244.00	162.03	161.98	566.41	566.41	603.01	603.0	288.55	288.42
$^PQ_3$	324.42	324.46	152.76	152.92	70.47	70.49	475.28	475.40	511.50	511.3	196.75	196.75
$^PQ_4$	305.77	a	134.38	134.37	51.96	51.78	456.34	456.21	492.69	492.5	178.26	b
$^PQ_5$	286.91	286.93	115.97	115.91							159.80	b
$^PQ_6$	268.02	267.97	97.55	97.57								

[a] Obscured by other bands.

[b] Q branches several wavenumbers wide.

creases because of the frequency factor

$$h\nu[1-\exp(-h\nu/kT)]$$

in the absorption coefficient.

The fact that ${}^{R}Q_6$ cannot be identified is probably a consequence of the perturbation of the $JKn\tau=J, 6, 1, 1$ energy level by the resonance discussed for the 11.43-cm^{-1} band. This would tend to shift ${}^{R}Q_6$ from its expected position of 233.4 cm^{-1} and cause it to merge with the broad absorption centered at 234.2 cm^{-1}.

The high asymmetry of the $n\tau=11$, 12 internal rotation level produces a narrowing of one of the central Q branches in the 116.51 cm^{-1} band, as it did in the 242.76 band. The computed J dependence of ${}^{R}Q_0$ of this band is; ${}^{R}Q_0(J)=125.67-7.2\times10^{-3}J(J+1)+6.2\times10^{-6}J^2(J+1)^2$. Therefore much of the absorption in the 123–125 cm^{-1} region is due to ${}^{R}Q_0$ as the former has approximately the predicted width and position.

The fact that there are no strong absorptions in the near vicinity of 143, 106, and 88 cm^{-1} that are otherwise not accounted for supports the 116.51-cm^{-1} band assignment and also, therefore, the 242.76 band assignment.

557.84-cm^{-1} Band

The 557.84-cm^{-1} band is of interest because it verifies that the 198.57-cm^{-1} band arises from the transition $n\tau=13\rightarrow21$ (and $14\rightarrow22$). It is characterized by fairly broad Q branches (1 to 2 cm^{-1} in half-width) of quite low intensity.

521.68-cm^{-1} band

The 521.68-cm^{-1} band has relatively narrow Q branches, but because of its low intensity the P side of the band is largely lost in the fine structure of the much stronger 370.70-cm^{-1} band. The absorption at 530.4 cm^{-1} is due to ${}^{R}Q_0$ which again is unusually narrow because the $JKn\tau=J$, 0, 1, 1 level is involved. The computed J dependence of ${}^{R}Q_0$ is ${}^{R}Q_0(J)=530.7-4.2\times10^{-3}J(J+1)+6.6\times10^{-6}J^2(J+1)^2$.

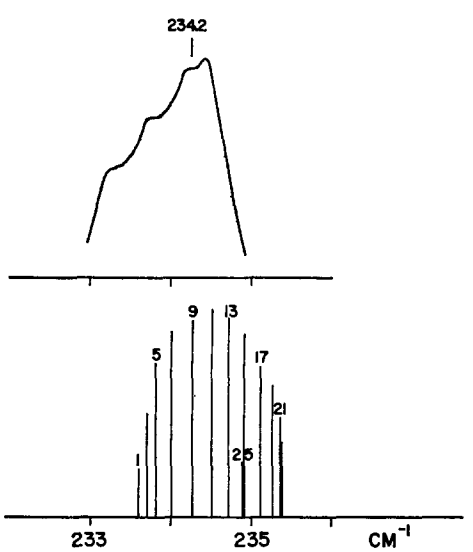

FIG. 7. Observed and calculated shape of ${}^{P}Q_1$ of the 242.76 cm^{-1} band.

TABLE X. Calculated relative band intensities.

Band	Intensity
242.76 cm^{-1}	2.01
116.51	0.62
370.70	1.00
198.57	0.37
557.84	0.16
521.77	0.09
206.60	0.19
223.6	0.09

The seven bands discussed above account for nearly all major absorptions with the notable exceptions of the strong absorptions at 251.3 and 269.4 cm^{-1}. The other band assignments demand that the transition $n\tau=21\rightarrow23$ ($22\rightarrow24$) occur at 206.60 cm^{-1}, and it is therefore in a position to contribute to these absorptions.

Table X lists the relative band intensities computed from the dipole-moment matrix elements and the appropriate frequency and Boltzmann factors. The 206.60-cm^{-1} band is predicted to have one-half the intensity of the 198.57-cm^{-1} band, and therefore is probably not sufficient to account for all of the absorption at 251.3 and 269.4 cm^{-1}. However, part of the absorption at 251.3 cm^{-1} may be due to ${}^{R}Q_7$ of the 116.51-cm^{-1} band which is calculated to occur at 251.0 cm^{-1}. In regard to the absorption at 269.4 cm^{-1}, it is interesting to note that if the transition $n\tau=23\rightarrow31$ ($24\rightarrow32$) occurred at 224.6 cm^{-1} instead of at the predicted 223.6 cm^{-1}, then ${}^{R}Q_2$ of this band would occur at 269.4 cm^{-1}. There is a good possibility that this is the case since the band observed at 206.60 cm^{-1} is predicted at 206.0 cm^{-1}. According to Table X, the 224.6-cm^{-1} band should have one-half the intensity of the 206.60-cm^{-1} band.

V. MICROWAVE SPECTRUM OF H_2O_2

Massey *et al.*[3,4] report 10 microwave lines for hydrogen peroxide between 11 000 and 40 000 Mc/sec, four of which have well-observed Stark effects. These four frequencies are given in Table XI.

The Stark field and the microwave electric field are both along the space-fixed Z direction in the experiment and hence, the selection rule for the quantum number M is $\Delta M=0$. The Stark shifts have the form $\Delta\nu=\epsilon^2[A-BM^2]$, where A and B are constants for a given transition and where ϵ is the strength of the Stark field. The observed Stark-effect coefficients for lines ν_1, ν_2, ν_3, and ν_4 are given in Table XII. To limit decomposition of the hydrogen peroxide vapor, Massey and Bianco maintained a pressure of 0.1 mm Hg in the absorption cell. At this pressure the microwave linewidths are several megacycles per second, and for this reason it was not possible to completely resolve the Stark patterns and unambiguously determine the maximum J in the transition, J^*, for lines ν_3 and ν_4. Several

TABLE XI. Four microwave lines of H_2O_2.

Line	Observed frequency (Mc/sec)	Remarks
ν_1	14 829.5±0.2	Quadratic Stark effect, $J^{*a}=1$
ν_2	37 517.6±0.2	Quadratic Stark effect, $J^*=2$
ν_3	22 054.5±0.2	Quadratic Stark effect, $J^*\geq 7$, $\Delta J=1$
ν_4	27 639.6±0.2	Quadratic Stark effect, $J^*\geq 7$, $\Delta J=1$

[a] J^* is the larger of the two values of J involved.

TABLE XII. The Stark effect in H_2O_2.

Line	Stark effect (Mc/sec)		Ratio B/A
ν_1	$\Delta\nu_1=\epsilon^2 29.09\times10^{-6}$[a]	...	$J^{*b}=1$
ν_2	$\Delta\nu_2=\epsilon^2[6.88-4.25M^2]\times10^{-6}$	0.618	$J^*=2$
ν_3	$\Delta\nu_3=\epsilon^2[5.65-0.0874M^2]\times10^{-6}$	0.01547	$J^*\geq 8$
	$=\epsilon^2[6.07-0.0727M^2]$	0.01198	≥ 9
	$=\epsilon^2[6.47-0.0623M^2]$	0.00964	≥ 10
ν_4	$\Delta\nu_4=\epsilon^2[4.18-0.0537M^2]\times10^{-6}$	0.01284	$J^*\geq 8$
	$=\epsilon^2[4.49-0.0459M^2]$	0.01022	≥ 9
	$=\epsilon^2[5.10-0.0356M^2]$	0.00698	≥ 10

[a] ϵ in volts per centimeter.
[b] J^* is the larger of the two values of J involved.

possible Stark-effect equations for ν_3 and ν_4 are shown with the minimum allowable value of J^* corresponding to each.

Massey's identification of lines ν_1 and ν_2 as internal-rotation ground-state transitions is confirmed by the analysis of far-infrared spectrum. In the notation of this investigation lines ν_1 and ν_2 are the transitions ν_1: $JKn\tau=1, 1-, 0, 2\rightarrow0, 0, 0, 4$ and ν_2: $JKn\tau=1, 0, 0, 4\rightarrow2, 1-, 0, 2$. The internal rotation ground-state splitting, E_{04}-E_{02}, is calculated to be 11.434 cm^{-1} in agreement with the far-infrared data. This splitting is computed using the values of the internal-rotation matrix elements given in Table VI and the experimental frequencies $\nu_1=14\,829$ Mc/sec and $\nu_2=37\,517$ Mc/sec.

Because the unknown vibration-internal-rotation interactions, which are due to the dependence of the inertial constants and the potential parameters V_1, V_2, ... upon the vibrational degrees of freedom, may give contributions of several thousand megacycles per second to energy levels with $J\geq8$, it is not possible to identify lines ν_3 and ν_4 by comparing calculated and observed frequencies. Since the Stark splittings can be predicted with an accuracy of several percent, they are used to select lines ν_3 and ν_4 out of 20 possible transitions having about the correct frequencies. The Stark-effect Hamiltonian is $-\mu_0\cos(x/2)\cos(x', Z)$ since the electric-dipole moment of the molecule, $\mu(x)=\mu_0\cos(x/2)$, is along the molecule-fixed x' axis and the Stark field is along the space-fixed Z axis. The form of the computed Stark-effect frequency shifts is $\Delta\nu=\epsilon^2\mu_0^2[A'-B'M^2]$.

As lines ν_1 and ν_2 are identified, their Stark-effect data are used to calculate the value of μ_0. The results are $\mu_0=3.15\pm0.05$ D for Line ν_1 and $\mu_0=3.24\pm0.05$ D for Line ν_2. In comparing the theoretical Stark effects of the possible transitions with the observed Stark effects of ν_3 and ν_4 the value of μ_0 as well as the ratio B/A can be used. The only candidates that fit both numbers are ν_3: $JKn\tau=8, 6\pm, 1, 1\rightarrow7, 5\mp, 1, 3$ and ν_4: $JKn\tau=8, 5\pm, 1, 3\rightarrow9, 6\mp, 1, 1$. Both transitions are effectively degenerate doublets because, for example, the asymmetry splitting of the $K=5\pm$ levels is estimated to be 0.000001 Mc/sec which is unobservable even in the microwave region. The relative intensities of the four lines are calculated and the H_2O_2 microwave results are summarized in Table XIII.

Since the Stark-effect matrix element of $\cos(x/2)$ for the ground state ($n=0\rightarrow0$) lines ν_1 and ν_2 has a value much different than the value for the first excited-state ($n=1\rightarrow1$) lines ν_3 and ν_4, the good agreement in μ_0 indicates that the hypothesis $\mu(x)=\mu_0\cos(x/2)$ is sound.[15] The identification of lines ν_3 and ν_4 as first excited-state transitions is further evidence in support of the hindering potential and internal-rotation energy-level structure determined by the analysis of the far-infrared spectrum.

VI. MICROWAVE SPECTRUM OF DEUTERATED HYDROGEN PEROXIDE

Massey, Beard, and Jen[16] have observed approximately 130 microwave spectral lines between 11 000

TABLE XIII. Identification of four H_2O_2 microwave lines.

Line	Observed frequency (Mc/sec)	Initial state				Final state				B/A observed	B/A calculated	μ_0 (D)	Relative intensity
		J	K	n	τ	J	K	n	τ				
ν_1	14 829.5	1	1−	0	2	0	0	0	4	...	...	3.15	0.035
ν_2	37 517.6	1	0	0	4	2	1−	0	2	0.618	0.624	3.24	1.00
ν_3	22 054.5	8	6±	1	1	7	5∓	1	3	0.0155	0.0151	3.12	0.041
ν_4	27 639.6	8	5±	1	3	9	6∓	1	1	0.0128	0.0130	3.16	0.061

[15] In principle, the form $\mu(x)=\mu_0\cos(x/2)+\mu_1\cos(3x/2)+\cdots$ is possible, however within the limits of this investigation only the first term is needed.
[16] J. T. Massey, C. I. Beard, and C. K. Jen, J. Mol. Spectry. 5, 405 (1960).

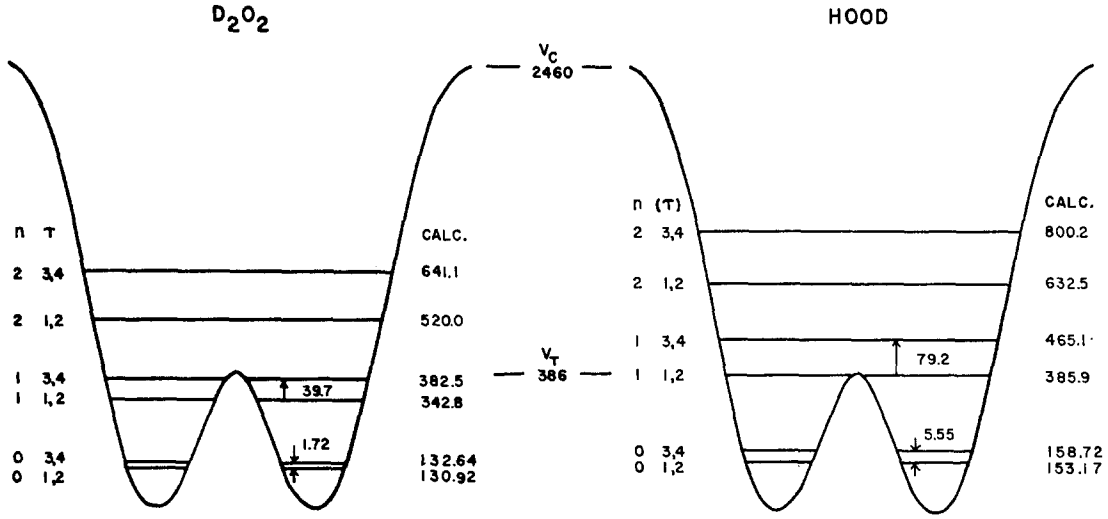

FIG. 8. The calculated internal-rotation energy levels of D_2O_2 and HOOD based on the H_2O_2 hindering potential function.

and 40 000 Mc/sec in a sample of deuterated hydrogen peroxide. This sample was a mixture of D_2O_2 and HOOD, and they were unable to assign any of the lines directly to either the D_2O_2 or HOOD species, nor were they able to identify the internal-rotation quantum numbers involved in the observed transitions. It was known, however, that none of the lines was attributable to H_2O_2. From observations of the Stark and Zeeman effects two series of the $\Delta J=0$ type were recognized. The observed frequencies of the individual lines of these series could be represented by the following empirical equations (in megacycles per second)

Series I:

$$\nu_I=38\,635-36.725J(J+1)-0.3\times10^{-6}J^6, \quad J\geq5, \quad (6.1)$$

Series II:

$$\nu_{II}=15\,250-371.2J(J+1)+0.220J^2(J+1)^2, \quad J\geq1. \quad (6.2)$$

In addition, Series I showed zero-field doubling of the frequencies for $J\geq11$. The empirical formula for this splitting (in megacycles per second) is

$$\Delta\nu_I=0.46\times10^{-8}J^8. \quad (6.3)$$

On the strength of the Stark data and the above empirical formulas Massey, Beard, and Jen identified Series I as arising from the transitions $\Delta J=0$, $K=4\leftrightarrow5$ with $J\geq5$ and Series II as arising from the transitions $\Delta J=0$, $K=0\leftrightarrow1$ with $J\geq1$. Series II changes sign for an intermediate value of J when the order of the energy levels is reversed.

The theory of internal rotation in D_2O_2 is identical to that for H_2O_2 with appropriate changes in the inertial parameters. HOOD, however, does not possess the symmetry of H_2O_2 and it is necessary to derive separately the HOOD Hamiltonian. The Hamiltonians of D_2O_2 and HOOD are discussed in detail in Appendix III.

The lower symmetry of HOOD makes itself felt in two ways. First, the K dependence of the internal-rotation wavefunctions and energies which arises through the boundary conditions is, in principle, more complicated. Secondly, the full Hamiltonian is no longer invariant under either of the symmetry operations C_{2x} or $\sigma(trans)$, so that the full Hamiltonian matrix no longer factors into four submatrices corresponding to wavefunctions of the $K+$, or $K-$, *trans* symmetry "s" or "a" type.

The internal-rotation wave equation has the same form in HOOD as in the symmetrical isotopic species: $[\alpha p_x'^2+V(x)]M(x)=EM(x)$, where $M(x)$ still has the form $M(x)=P(x)\exp(i\sigma x)$ with $P(x)=P(x+2\pi)$ and where $\sigma=-K(\frac{1}{2}-\omega)$. In the symmetrical molecules, H_2O_2 and D_2O_2, $\omega=0$; in HOOD the boundary conditions give $\omega=0.152$, $\sigma=-K(0.348)$. It might thus be expected that the HOOD internal-rotation energy levels are strongly K-dependent as in methyl alcohol. Unlike methyl alcohol, however, hydrogen peroxide and its isotope species have a large barrier to internal rotation which results in unobservable *cis* splitting of the lower internal-rotation energy levels and therefore in negligible K dependence for these levels. For this reason, it is possible to illustrate the $n=0$, 1, 2 internal-rotation energy levels of HOOD by one K-independent diagram similar to those for H_2O_2 and D_2O_2. The internal-rotation wave equations for both HOOD and D_2O_2 have been solved numerically under the assumption that the hindering potential is mass independent and is exactly the same in the three isotopic species.[17] The predicted internal-rotation levels for D_2O_2 and HOOD are shown in Fig. 8.

[17] The potential parameters $V(trans)$, $V(cis)$, and x_0 are effective potential parameters which include small mass dependent contributions from the vibration–internal-rotation interactions so that small corrections to the H_2O_2 potential parameters for the species D_2O_2 and HOOD are expected.

The quantum numbers n and τ retain their original meaning in the case of D_2O_2, but τ no longer refers to the symmetry type of the internal-rotation wavefunctions in HOOD as it did in H_2O_2. For convenience of comparison, the internal-rotation energy levels of HOOD are nevertheless labeled by $Kn\tau$ where $\tau=2$ (or 1) now refers to the lower of the two energy levels for a given n and K and $\tau=4$ (or 3) refers to the upper of the two levels for a given n and K.

The zeroth-order energies of D_2O_2 and HOOD are $E(JKMn\tau)=\beta_{n\tau}{}^{n\tau}J(J+1)+\nu_{n\tau}{}^{n\tau}K^2+E_{n\tau}$, where the values of $\nu_{n\tau}{}^{n\tau}$ for the ground states are $\nu(D_2O_2)=4.65$ cm^{-1} and $\nu(\text{HOOD})=6.23$ cm^{-1}.

Series I

Series I is assigned as the D_2O_2 transitions $JKn\tau=J$, $4\pm$, 1, $4\rightarrow J$, $5\pm$, 1, 2. A first excited-state transition in HOOD would fall in the microwave region for a change in K of $K=6\rightarrow 7$ which would require that Series I start with $J=7$ contrary to the empirical equation (6.1). Further evidence for the assignment of Series I to D_2O_2 transitions comes from the observed zero-field splitting due to the asymmetry of the molecule.

The Wang formula for the splitting of the energy levels of a slightly asymmetric rigid top may be used to estimate the zero-field splitting in the isotopic species D_2O_2 and HOOD if the contributions to the splittings by other ($n\neq 1$) internal-rotation energy levels are neglected and if the asymmetry parameter b is replaced by

$$\frac{\gamma_{n\tau}{}^{n\tau}}{\nu_{n\tau}{}^{n\tau}}+\frac{|\delta_{n\tau}{}^{n\tau}|^2}{2(\nu_{n\tau}{}^{n\tau})^2}.$$

The results are (in megacycles per second)

$$\Delta\nu_I(D_2O_2, K=4)=0.467\times 10^{-8}(J+4)!/(J-4)!,$$

$$\Delta\nu_I(\text{HOOD}, K=6)=\sim 2\times 10^{-20}(J+6)!/(J-6)!,$$

which are to be compared with the empirical formula (6.3). The D_2O_2 asymmetry-splitting formula gives asymmetry splittings about twenty percent larger than those observed by Massey. The J dependence of the D_2O_2 formula is J^8 in agreement with the observed empirical formula. In contrast, the HOOD splitting formula gives no observable asymmetry splittings for the observed values of $J(J\leq 21)$. Furthermore, the J dependence of the HOOD formula is J^{12} in strong disagreement with the empirical equation of Massey. On the basis of these comparisons, Series I is identified as the $JKn\tau=J$, $4\pm$, 1, $4\rightarrow J$, $5\pm$, 1, 2 D_2O_2 transitions.

The terms of the empirical formula for the D_2O_2 microwave Series I are predicted using the techniques of perturbation theory. The empirical terms $-D_JJ^2(J+1)^2-D_{JK}J(J+1)K^2-D_KK^4$ for D_2O_2 are estimated from the values obtained for H_2O_2 and are used in the theoretical prediction of the coefficients of Series I. The result (in megacycles per second) is

$$\nu_I=81\,000-16.4J(J+1)+0.005J^2(J+1)^2+1\times 10^{-8}J^3(J+1)^3.$$

The discrepancy between the observed and calculated constant terms of Series I is about 1.4 cm^{-1} in the first excited-state splitting of 40 cm^{-1}. A change in the height of the *trans* hill $V(trans)$ from the H_2O_2 value of 386 to 378 cm^{-1} for D_2O_2 adjusts the excited-state splitting to fit the constant term of Series I exactly. In principle, $V(cis)$ and x_0 could also be adjusted, but the one piece of information is insufficient to determine uniquely the corrections to all three potential parameters.

The discrepancy between the observed and calculated $J(J+1)$ coefficients is expected to arise from the unknown vibration–internal-rotation interaction terms. The order of magnitude of these terms could account for the 20 Mc/sec difference between theory and experiment. The $J^2(J+1)^2$ and J^6 terms are very uncertain from the experimental data and are difficult to discuss on the basis of the semirigid-model theory of this investigation.

Series II

By use of the Stark effect, Massey has identified Series II as a $\Delta J=0$, $K=0\rightarrow 1$ series. As in the case of Series I, there are two alternatives for the origin of Series II: $JKn\tau=J$, 0, 0, $4\rightarrow J$, 1+, 0, 2 transitions in D_2O_2 and $JKn\tau=J$, 0, 0, $4\rightarrow J$, 1, 0, 2 transitions in HOOD. The predicted constant term of the series for D_2O_2 is approximately 90 000 Mc/sec while the predicted constant term for HOOD is approximately 20 000 Mc/sec. The observed constant term is 15 250 Mc/sec. A change of 0.16 cm^{-1} in the predicted 5.55 cm^{-1} splitting of the $n=0$ levels of HOOD leads to agreement between the predicted and observed values of this constant term. On the other hand, a change of 2.5 cm^{-1} in the predicted 1.73 cm^{-1} splitting of the $n=0$ levels in D_2O_2 is required if the series has its origin in the D_2O_2 isotopic species. Such a large percentage change in the ground-state internal-rotation splittings could be effected only through large percentage changes in the D_2O_2 hindering potential parameters. Since vibration–internal-rotation effects are expected to lead only to minor changes in the effective hindering-potential parameters, the origin of Series II is assigned to the HOOD transitions.

Calculations of the energy levels of HOOD by diagonalization of the full Hamiltonian are carried out as in H_2O_2 and D_2O_2 with the exception that the Hamiltonian matrix no longer factors into four submatrices corresponding to the symmetries K^+, K^-, *trans* symmetry s, or a. The $K=0$ level of HOOD is nondegenerate. The perturbation corrections to the zeroth-order energies include sums over four times as many states as in the symmetrical molecular species, but those states which were excluded by symmetry in

H_2O_2 and D_2O_2 give negligible contributions to the $K=0$ energy

In principle, the two perturbed diagonal matrix elements for $|K|=1$ could be different for a molecule with the symmetry of HOOD. In HOOD, however, the difference between the $K=+1$ diagonal matrix element and the $K=-1$ diagonal matrix element is negligible compared with the off-diagonal element, so that the stabilized eigenfunctions are given to very good approximation by

$$\Psi_{K=1\pm}=(1/\sqrt{2})[\Psi_{K=1}\pm\Psi_{K=-1}],$$

that is, the symmetry of these HOOD eigenfunctions is for purposes of calculation the same as that required in the case of H_2O_2. The predicted terms of Series II (in megacycles per second) are

$$\nu_{II}=20\,300-381J(J+1)+0.18J^2(J+1)^2.$$

The 5000 Mc/sec discrepancy between the observed and calculated constant terms of Series II is ascribed to small differences in the effective hindering-potential parameters of H_2O_2 and HOOD. A change of $V(trans)$ from 386 cm^{-1} for H_2O_2 to 381 cm^{-1} for HOOD leads to a fit of this constant term. The agreement of the observed and calculated coefficients of the $J(J+1)$ term is within 3%. The major contribution to this term arises from the asymmetry splitting of the $K=\pm1$ levels, and hence the unknown vibration–internal-rotation effects give a small percentage contribution to the term. Their order of magnitude is expected to be similar to that of the analogous term in D_2O_2 and can therefore be estimated from the differences between the observed (−36.7 Mc/sec) and theoretical (−16.4 Mc/sec) coefficients of the $J(J+1)$ terms of Series I. Since this difference of about 20 Mc/sec is of the same order as the difference between the predicted and observed $J(J+1)$ coefficients of Series II, the agreement between theory and experiment is satisfactory. The predicted $J^2(J+1)^2$ term is also in good agreement with the observed term giving further confidence in the assignment of Series II.

The assignment of the observed $\Delta J=0$ series to the transitions $JKn\tau=J$, $4\pm$, 1, $4\rightarrow J$, $5\pm$, 1, 2 in D_2O_2 (Series I) and $JKn\tau=J$, 0, 0, $4\rightarrow J$, $1+$, 0, 2 in HOOD (Series II) gives further confirmation of the hindering-potential parameters determined by the far infrared spectrum analysis. The changes in the value of $V(trans)$ necessary to fit the constant terms of Series I and II are small as expected and show a reasonable progression from H_2O_2 to D_2O_2:

H_2O_2: $V(trans)=386$ cm^{-1},

HOOD: $=381$,

D_2O_2: $=378$.

APPENDIX I. INERTIAL PARAMETERS

The inertial parameters which appear in the kinetic-energy expression of the hydrogen peroxide molecule [Eq. (3.1)] are

$$A(x)=A_0+A'\sin^2(x/2),$$

$$B(x)=(A_0+C_0)-C'\sin^2(x/2),$$

$$C(x)=C_0+C'\sin^2(x/2),$$

$$D(x)=D_0\sin(x/2),$$

$$F(x)=D_0\cos(x/2),$$

$$G(x)=A'-C'\sin^2(x/2),$$

where the constants A_0, A', C_0, C', and D_0 are given in terms of the OO distance r_1, the OH distance r_2, the OOH angle γ, the oxygen nuclear mass M, and the hydrogen nuclear mass m by the expressions

$$A_0=\tfrac{1}{2}Mr_1^2+2m(\tfrac{1}{2}r_1-r_2\cos\gamma)^2,$$

$$A'=2m(r_2\sin\gamma)^2,$$

$$C_0=[2mM/(m+M)](r_2\sin\gamma)^2,$$

$$C'=[2m^2/(m+M)](r_2\sin\gamma)^2,$$

$$D_0=-2m(r_2\sin\gamma)(\tfrac{1}{2}r_1-r_2\cos\gamma).$$

For the values $r_1=1.475$ Å, $r_2=0.950$ Å, and $\gamma=94.8°$ (Ref. 6) the values of the constants are in units of 10^{-40} g-cm^2: $A_0=31.114$, $A'=2.998$, $C_0=2.820$, $C'=0.178$, and $D_0=-2.587$.

APPENDIX II. HINDERING POTENTIAL FUNCTION

The hindering-potential function is

$$V(x)=V_0+V_1\cos x+V_2\cos 2x+V_3\cos 3x,$$

where the V_i are constants. The relations between V_0, V_1, V_2, and V_3 and the parameters $V(cis)$, $V(trans)$, and x_0 are

$$V_0=G[(V_c+V_t)(\sin^2x_0+2\cos^4x_0)+(V_c-V_t)2\cos^3x_0],$$

$$V_1=G[(V_c-V_t)(\tfrac{3}{2}-\tfrac{9}{2}\cos^2x_0+2\cos^4x_0)-(V_c+V_t)\cos x_0],$$

$$V_2=G[(V_c+V_t)(1-3\cos^2x_0)-(V_c-V_t)2\cos^3x_0],$$

$$V_3=G[(V_c+V_t)\cos x_0+(V_c-V_t)(\tfrac{1}{2}+\tfrac{1}{2}\cos^2x_0)],$$

where $G=[4\sin^4x_0]^{-1}$. V_0 is not spectroscopically observable and is introduced merely for convenience to make $V(x_0)=0$.

APPENDIX III. HAMILTONIANS OF D_2O_2 AND HOOD

The semirigid-model assumptions used in the derivation of the H_2O_2 Hamiltonian are used in the D_2O_2 and

HOOD Hamiltonian derivations. The Hamiltonian of D_2O_2 is identical to that of H_2O_2 with new inertial parameters (in cm^{-1}):

$$\beta(x)=0.772+0.00692\cos x+0.00241\cos 2x+\cdots,$$

$$\nu(x)=4.598-0.135\cos x+0.0134\cos 2x+\cdots,$$

$$\gamma(x)=0.00184+0.0550\cos x+0.000979\cos 2x+\cdots,$$

$$\alpha(x)=21.277+0.190\cos x+0.0960\cos 2x+\cdots,$$

$$\delta(x)=0.146\sin^3(x/2)+\cdots.$$

These numbers are based on the structural distances and angle of Redington *et al.* for the H_2O_2 molecules.

The derivation of the HOOD Hamiltonian is similar to that for H_2O_2. The Hamiltonian is

$$H=\tfrac{1}{2}I_{\alpha\beta}P_\alpha P_\beta + I_{x4}p_xP_x+I_{y4}p_xP_y+I_{z4}p_xP_z+\tfrac{1}{2}I_{44}p_x^2+V(x),$$

where x is the internal angle defining the relative orientation of the two bars: OH and OD. p_x is the momentum canonical to x and P_x, P_y, and P_z are the components of the total angular momentum along the molecule-fixed axes. Repeated indices are summed over from 1 to 3. To eliminate the interaction terms p_xP_i a contact transformation of the Hamiltonian is effected. The transformation has the form

$$p_x=p_x'-k_\alpha(x)P_\alpha', \qquad P_i=a_{i\alpha}(x)P_\alpha',$$

where the a_{ij} satisfy the coupled differential equations

$$\partial a_{ij}/\partial x=-\epsilon_{i\nu\sigma}(I_{\nu 4}/I_{44})a_{\sigma j},$$

and where $\epsilon_{ijl}=1$ for cyclic permutations and -1 for noncyclic permutations and 0 if any two indices are equal. In terms of the a_{ij} the $k_i(x)$ are

$$k_i(x)=(I_{\alpha 4}/I_{44})a_{\alpha i}(x).$$

The transformed Hamiltonian is

$$H=\beta(x)P'^2+\nu(x)P_z'^2+\gamma(x)[P_x'^2-P_y'^2] +\rho_1(x)[P_x'P_y'+P_y'P_x']+\rho_2(x)[P_y'P_z'+P_z'P_y'] +\rho_3(x)[P_z'P_x'+P_x'P_z']+\alpha(x)p_x'^2+V(x),$$

where

$$\beta(x)=\beta_0+\beta_1\cos x+\cdots,$$

$$\nu(x)=\nu_0+\nu_1\cos x+\cdots,$$

$$\gamma(x)=\gamma_0+\gamma_1\cos(1+2\omega)x+\gamma_2\cos(1-2\omega)x+\cdots,$$

$$\rho_1(x)=\gamma_0+\gamma_1\sin(1+2\omega)x-\gamma_2\sin(1-2\omega)x+\cdots,$$

$$\rho_2(x)=\rho_1\sin(\tfrac{1}{2}+\omega)x+\rho_2\sin(\tfrac{1}{2}-\omega)x+\cdots,$$

$$\rho_3(x)=\rho_1\cos(\tfrac{1}{2}+\omega)x-\rho_2\cos(\tfrac{1}{2}-\omega)x+\cdots,$$

$$\alpha(x)=\alpha_0+\alpha_1\cos x+\alpha_2\cos 2x+\cdots,$$

and where ω is an angle determined by the contact transformation to eliminate the three p_xP_i interaction terms ($\omega=0.152$ rad). As $\omega\to 0$ the form of the HOOD Hamiltonian returns to that of H_2O_2 and D_2O_2. The values of the constants based on the Redington structural parameters are (in cm^{-1}): $\beta_0=0.817$, $\beta_1<0.002$, $\nu_0=6.179$, $\nu_1=-0.108$, $\gamma_0<0.001$, $\gamma_1=0.016$, $\gamma_2=0.032$, $\rho_1=0.023$, $\rho_2=0.046$, $\alpha_0=30.605$, $\alpha_1=0.228$, $\alpha_2=0.0658$. The matrix elements of the total Hamiltonian using as basis functions the symmetric-top eigenfunctions multiplied by the internal-rotation eigenfunctions are

$$H_{JKn\tau}{}^{JKn\tau}=\beta_0J(J+1)+\left[\nu_0+\nu_1\int dx P^*_{Kn\tau}\cos x P_{Kn\tau}\right]K^2+E_{n\tau},$$

$$H_{JKn\tau}{}^{J,K+1,n'\tau'}=\tfrac{1}{2}(2K+1)[(J-K)(J+K+1)]^{\frac{1}{2}}\times\int dx P^*_{Kn\tau}[\rho_1e^{-ix}-\rho_2]P_{K+1,n'\tau'},$$

$$H_{JKn\tau}{}^{J,K+2,n'\tau'}=\tfrac{1}{2}[(J-K)(J-K-1)(J+K+1)(J+K+2)]^{\frac{1}{2}}\times\int dx P_{Kn\tau}[\gamma_1e^{-i2x}+\gamma_2]P_{K+2,n'\tau'},$$

where the quantity $P_{Kn\tau}(x)$ is the periodic portion of the internal-rotation wavefunction:

$$M_{Kn\tau}(x)=\exp(i\sigma x)P_{Kn\tau}(x), \qquad P_{Kn\tau}(x)=P_{Kn\tau}(x+2\pi).$$

The value of σ is determined by the boundary conditions on the molecular wavefunctions as in H_2O_2. For H_2O_2 and D_2O_2 the value of σ is $-K/2$. This value is corrected in the case of HOOD to $\sigma=-K(\frac{1}{2}-\omega)$. It is noted that ω does not appear in the matrix element of the total Hamiltonian because the ω dependence of the internal-rotation wavefunctions exactly cancels the ω dependence of the Hamiltonian when the matrix elements are formed.